Note # 2. Proposal to Build Forward Calorimeters for the RHIC Heavy IonExperiments

Edmundo J. Garcia-Solis, for the ZDC Collaboration:

BNL, Frankfurt, IHEP-Protvino, Maryland, Texas-AMU

March 12, 1998

Abstract

Two mechanisms for forward correlated neutron emission in heavy ion collisions motivate the construction of compact hadron calorimeters to be placed downstream of interaction regions at RHIC. It is intended to build a standard detector for all RHIC experiments. This proposal describes the performance requirements, the simulation results, and the options for a baseline design. Also, included in this paper is the discussion of the prototype test run performed at CERN in fall 97.

1 Introduction

If the number of forward neutrons can be measured along both beam directions in RHIC heavy ion collisions, this information will be used both for monitoring Luminosity through the Correlated Coulomb Dissociation rate and as a tool for measuring centrality of hadronic collisions on an event-by-event basis.

What is needed for luminosity monitoring is a clean reaction with straightforward detector acceptance. The photonuclear process proposed here results in coincident beam energy neutron emission along each beam direction. The RHIC collider design is compatible with detectors covering $\sim 100\%$ of the required solid angle with $\sim 10 \cdot 10\ cm^2$ area. Similar detectors have been exposed in beam tests and a fixed target heavy ion experiment.

What is needed for event characterization is a measure of the nuclear overlap in a hadronic collision. In fixed target heavy ion experiments, small aperture **Z**ero **D**egree **C**alorimeters (**ZDC**) are used to measure centrality via the disappearance of beam energy spectators. At a collider, beam energy fragments follow the beam orbit but unbound protons and neutrons will leave the beam tube after the first bending magnet (Z/A of the beams is $\sim \frac{1}{2}$). Since it is intended to measure only neutrons with the RHIC calorimeters, a short experiment was performed at CERN to verify that the fluctuations in spectator fragmentation did not wash out the effectiveness of recording solely neutron spectators.

2 Mutual Coulomb Dissociation and Luminosity Monitoring

The Coulomb dissociation of a single beam nucleus in collisions of identical beam species has already been considered in some detail for RHIC [3],[2]. This process is of interest because it is one of the limiting factors affecting beam lifetime. However, for luminosity monitoring this is not considered an effective diagnostic tool since it is not easily distinguished from "single beam" backgrounds. On the other hand, a simple extension of the Weizsacker-Williams treatment of this process reveals a large component of dissociation as mutual [1]. The coincident detection of neutrons along each beam direction makes the process cleaner and suitable for Luminosity monitoring.

The cross section for heavy ion dissociation may be accurately expressed in terms of the (experimentally known) photodissociation cross sections, $\sigma_{ph}(\omega)$, of the same nucleus over an appropriate range of photon energies.

$$\sigma_{dis} = \frac{2\alpha Z_p^2}{\pi\gamma^2}\int d\omega\omega\sigma_{ph}(\omega)\int_{b_0}^{\infty} b\,db K_1^2(\frac{b\,\omega}{\gamma}). \tag{1}$$

In order to calculate the mutual dissociation cross section for the two colliding nuclei, one can define a dissociation probability, P(b), as a function of impact parameter b

$$\sigma_{dis} = 2\pi\int_{b_0}^{\infty} P(b) b\ db. \tag{2}$$

Then inverting the order of integration in Eq. (1) we have

$$P(b) = \frac{\alpha Z_p^2}{\pi^2\gamma^2}\int d\omega\omega\sigma_{ph}(\omega)K_1^2(\frac{b\,\omega}{\gamma}). \tag{3}$$

Neglecting, for the moment, the fact that P(b) approaches unity at grazing impact in our case. It is given instead a first order expression for correlated dissociation, $\sigma_{cd}^{(1)}$, which is subsequently corrected to preserve unitarity. Then

$$\sigma_{cd}^{(1)} = 2\pi\int_{b_0}^{\infty}\Big[P(b)\Big]^2 b\ db, \tag{4}$$

which may be evaluated numerically using the data on $\sigma_{ph}(\omega)$. As discussed in ref.[1], the resulting cross sections are sensitive to impact parameter cutoff (b_0) at the level of 10 to 15%. Taking b_0 = 15 fermi, we found σ_{cd} =3.9 barns at RHIC top energy with gold beams and 7.2 barns at LHC top energy with Pb beams.

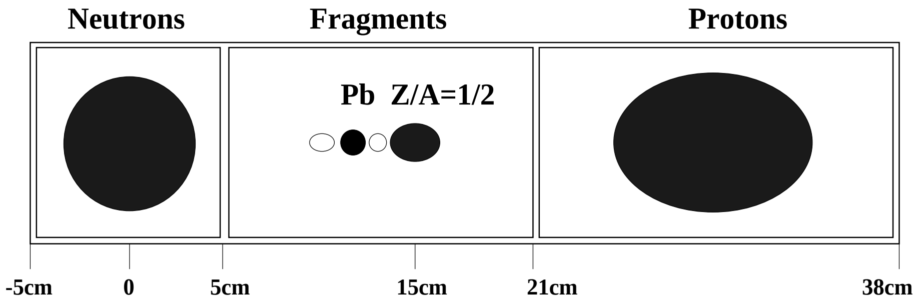

Figure 1: Fragment distribution at the forward calorimeter in the NA49 test.

3 Experimental Considerations, Detector Requirements

The spectrum of emitted neutrons determines the design criteria for the luminosity monitor detectors. Their lab energy and angular distributions were calculated from photonuclear data. More than half of the inclusive dissociation cross section results in single neutron emission with a lab energy spread of $\sigma \leq 10\% \times E_{beam}$. So the measured line width will be determined by the detector resolution which has been required to be $\leq 20\%$ @ 100 GeV. The angular distribution is limited to a cone of 1.4 mr opening angle at RHIC top energy (± 2.5 cm at the ± 18 m location of the detectors in RHIC). The neutron calorimeter response should be flat over this area. The final requirement on the 2 calorimeters comes from the possibility of time difference measurement to locate the interaction point. It has been required to be $\sigma_t = 300$ psec.

4 Event Characterization with a Neutron Calorimeter

In a special run of NA49 [4], "centrality" of 158 GeV/n Pb + Pb target collisions was measured simultaneously using a large angle "ring" calorimeter and a forward (ZDC) calorimeter, $\sim$ 25 m downstream of the target. A magnet between the target and ZDC separated the fragments so that different species could be measured independently. The resulting geometry, shown in Fig.1, is identical to the configuration around the RHIC neutron detector location. The "fragment" region corresponds to the orbit of one stored beam.

Preliminary results from the run confirm the sensitivity of the neutron calorimeter to "centrality". A large neutron multiplicity ($\sim$ 10) is observed even in the most central events.

4.1 Role of EM energy Measurements

It has been also considered the possibility that coherent bremsstrahlung radiation of photons from nuclear collisions could provide a useful measure of collision impact parameter. This process, discussed by Bjorken and McLerran [17, 18] provides centrality measurement because of the Z^2 dependence of the radiation intensity on the overlap region in a collision. Initial estimates [18] placed the the total radiated energy at 500 GeV per hemisphere in a RHIC central collision. This intensity would overwhelm the photon background from meson decay in the very forward (≤ 2 mr.) region.

However these measurements would not become accessible by addition of an EM compartment to the proposed neutron calorimeter. First of all, the angular distribution of radiation extends well beyond the coverage of the zero degree detector. Secondly, the total radiated energy has recently been reevaluated and a much lower flux is now expected [19]. Measuring this process will require a specialized detector and the likelihood that it could serve as an aid in event characterization seems low.

5 Available space for Forward Calorimeter

This section describes the space constraints in the region downstream of the DX magnets at RHIC, along what is referred to as the zero degree line. Particular attention will be given to the space available for a detector centered on this zero degree line, downstream of the DX magnet. This region is of interest for detecting forward neutrons. Forward protons could also be detected downstream of DX since they have higher charge-to-mass ratio than the ion beams and would be swept out of the beamtube- however this option is not discussed here.

For reference, the DX magnets are warm bore, superconducting dipole magnets that reside on either side of the RHIC interaction regions (IR). The centers of these dipoles are located approximately 11.65 m on either side of the interaction point (center of IR hall). The total length of the DX magnet assembly, from flange to flange, is $\sim$ 6.11 m. The downstream end of the DX magnet is approximately 14.73 m from the interaction point. Following the DX magnet there is a bellows section of pipe with a diameter of $\sim$ 30.5 cm, and a length of $\sim$ 50 cm. In the present design this bellows is followed by a conical pipe. The diameter of this pipe starts at $\sim$ 30.54 cm on the end that attaches to the bellows, and increases along its length to a final diameter of 41.9 cm. The length of this conical pipe is $\sim$ 267 cm. The downstream end of this pipe is closed off with a plate that contains two 12.7 cm diameter holes, centered horizontally, with a distance of 22.2 cm between the centers of the holes. Individual 12.7 cm diameter beam pipes carry the incoming and outgoing beams from this point to flanges $\sim$ 1.7 m further downstream from the IR. The maximum possible distance between beampipes consistent with different machine operating configurations was calculated in RhicDet.Note#6 [15] and found to be 15 cm at the downstream end of the warm section. The distance between two beam pipes that attach to the plate at the end of the conical pipe is 9.5 cm in the current RHIC design (a revised figure of this region is in preparation). The angle that these pipes make with respect to the zero degree line is + and - about 18.7 mrad. The total distance from the interaction point (IP) to the dowstream face of the plate, at the end of the conical tube, is 17.85 m. If one goes 40 cm further downsteam from this plate, one gets to a point where the total distance between the two pipes is 11.0 cm. It is at this point, approximately 18.25 m downstream from the interaction point, where one could place a detector with a full width of something like 10 cm (allowing for 5 mm clearance on each side). These two beam pipes extend downstream for 1.3 m before both pipes encounter a flange. The distance between the two flanges at this point is 11.4 cm. About 30 cm past the start of these flanges one reaches a gate valve on each pipe. There is essentially no space between these gate valves, so this defines the maximum distance from the IP for a zero degree detector to end. Summarizing, the space available for a detector at zero degrees in the current RHIC design, starts at a minimum distance of 17.85 m from the IP, where one could place a detector with a width of 8.5 cm, if one were to start at 18.25 m from the IP one could place a detector with a width of 10 cm. The flanges, at a distance of 19.5 m from the IP constrain the width of a detector to maximum possible extent where one could place a detector.

6 Simulations,Calorimeter Design

The design choice is based on the simulation of performance of options fitting within the available transverse dimensions.

Unless otherwise specified, all cases are for Cerenkov fiber sampling with a 45^o tilt angle of absorber and fiber with respect to the beam direction. The reasons for this choice are given elsewhere [15]. The options were scoped by simulating with Geant the response to neutrons distributed over the front face of the calorimeter with a p_t distribution characterized by Fermi motion. In fact the p_t distribution for Mutual Coulomb Dissociation will be somewhat narrower and transverse leakage effects should be less severe.

Most of the ZDC special requirements are in, fiber numerical aperture(NA) and orientation, and photoelectron response for visible and for uv, and three readout devices, quartz and borosilicate glass pmts and HPDs. The code has been checked on all of the experimental ZDC data for EM and Hadronic response listed in the references below.

The results for absorber choice with our geometrical restrictions in order are: uranium, tungsten, tantalum, lead and copper is last. All are viable, but lead and copper cannot make the energy resolution target of 20% at 100 GeV. The factors considered, in rough order of deterioration of the energy resolution(or at least ease of doing something about it) are:

1. shower leakage, mainly transverse due to the 10cm dimension
2. intrinsic binding energy fluctuations, mainly pi-zero fluctuations
3. sampling fluctuations
4. photon statistics

6.1 Shower Leakage

Use of uranium or tungsten brings the shower Cherenkov-sensitive shower leakage under control and switches the 1) and 2) priorities. It is near the top because it costs money. Use of the dense absorbers also makes a more compact structure longitudinally and it is more certain that a 8λ structure will fit in the final RHIC design. Uranium is best for energy resolution because of a smaller e/mip and thus a better e/h ratio as described later. Uranium may be a bit cheaper than tungsten, even with $300/hr machine shop time, but we almost certainly cannot use it because of environmental reasons.

The short attenuation length of tungsten helps the transverse containment, but the situation is a little more complicated and hurts the usefulness of copper more than expected. The fiber numerical aperture is important (the whole method depends on it) so NA=0.22 is needed here. But it must be must remember that the shower dimension shrinkage over dE/dX devices is 1/2-1/3, at the 80-90 % containment radii, and still is in conflict with the 10 cm dimension.

The following table shows results of our calculations (which whenever possible have been compared to data) . Copper is apparently slightly worse than lead. Except where noted, the results are for 100 GeV protons, 200 micron NA=0.22 quartz fiber, uv +vis light XP2020Q pmts and the 45 degree tilted plates.

ABSORBER	THICK(cm)	R(90%) cm	LEAK
CU	1.4	7.87	26
Cu	1.0	7.93	27
W	0.35	4.59	8
Pb	0.56	7.91	26
U	0.32	4.92	9
Cu	1.0	8.75	30

The energy resolution can be calculated as given below with various components contributing to the resolution 1-4 previously. The sigma values are given separately except for leakage which is integrated with sampling and photoelect. statistics. The esoultion scales with 1/SQRT(E) to this point, with little constant term. Binding energy fluctuations may need more work and may be underestimated somewhat. These are dominated by pi-zero statistics and will not scale as 1/SQRT(E), and are the major source of the constant term in sigma/E.

ABSORBER	THICK (cm)	SIG samp	SIG pe	SIG s+pe+leak	e/h SIG	BE	SIG-TOTAL E-resol
Cu	1.4	7.0%	9.8%	24%	5.3	17.6%	29.8%
Cu	1.0	5.8	7.5	19.3	5.2	17.7	27.4
W	0.35	4.6	5.6	9.7	2.9	14.4	17.3
Pb	0.56	4.4	7.4	17.5	2.5	13.6	22.2
U	0.32	4.2	5.5	9.4	2.1	12.6	15.7
W***	1.0			8.5	1.0	2.5	8.9

W*** is a tungsten- liquid scintillator design, included for perspective The resolution for lead would be worse because an 8λ structure would not fit. Most plate thicknesses are 1X, except for Cu, where it makes no difference i.e. the 1.0 cm has no effect on e/h.

The 0 degree fiber e/h intrinsic ratio value for Cu is 7.3, in good agreement with estimates given in Wigman's 1995 NIM paper. The e/h ratios for Pb are 3.5 for 0 deg. fibers and 2.5 for 45 degrees as given in the table. These disagree with fits to simulated data in NIM A361(1995) p 170.

Having selected Tungsten as an optimal choice for absorber material it is possible to modify the plate thickness and fiber thickness in order to select among ready options for plates which are available "off the shelf". It was proposed to work with 2.5mm plates. These are the results:

entry#	thick(mm)	Samp res	pe res	s+pe+leak	e/h	BE res	total
1	3.5	4.6	5.7	9.7	2.9	14.4	17.3
2	5.0	5.5	5.7	10.5	2.8	14.3	17.8
3	5.0	5.5	4.8	9.6	2.8	14.3	17.2
4	2.5	3.9	4.8	9.2	3.8	18.1	20.2

The first entry should be identical to the previous 3.5 mm W, 200 micron fiber 10 cm dimension and 8λ deep. The second entry only increases the plate thickness to 5.0 mm and the third entry also increses the fiber to 400 micron. The fourth entry uses 2.5 mm tungsten and 200 micron fiber.

Entry 1 has 155 layers, entries 2,3 109 layers, entry 4 has 217 layers. If anything, the binding energy term is underestimated . The bonding of two 2.5 mm plates with a radiation resistant agent is our choice for the design given below.

One sees that the intrinsic fluctuations dominate, and that is the reason to to try to reduce the plates, i.e. reduce e/h.

6.2 Fiber Choice

The original simulations assumes the use of acerenkov fiber with a small numerical aperture (NA=0.22). These fibers are availble commercially with Quartz core. However, for the RHIC application a dose over a 10 year period is expected to be in the few 10^4 range. Thus this was not the main argument for using or not the quartz fiber. Quartz fiber is generally more expensive and more difficult to polish and handle.

Instead of Quartz fiber, plastic fiber could be used. It appeared feasible to make low index PMMA core/PMMA clad fiber, however it has not been found yet a commercial source for this fiber. It is not known if low NA polystyrene core fiber is available. The PMMA fiber is just marginally acceptable for our application, having typical induced attenuation of $\leq$ 1dB/m at doses of 10^4 rads. Finally, the PS fiber is another feasible choice since it is more radiation hard than the PMMA fiber by at least an order of magnitude in the 400 nm to 500 nm wavelength region [16].

The pricing assumption is 50 cents/meter for 0.5 mm diameter fiber, provided the continuation of the search for vendor quotes for fiber with a low numerical aperture. The assumed photostatistics with the fiber and photodetector combination is based on lab tests with cosmic muons. It was found a yield of 0.5 photoelectrons per mm.

7 Costs and Design Parameters

The costing table assumes that the calorimeter module will be read-out by two independent photomultipliers. A 2" PMT for the readout of the 1st 2 λ and a 5" PMT to readout the remaining 6 λ. The first PMT is likely to give better timing resolution because the calorimeter volume is more compact. It was also found that a single 5" PMT could readout the full fiber area.

Either of these options can be calibrated with high energy minimum ionizing muons. After these are used for gain balance the position of the 1 neutron energy peak can also be predicted and final calibration will be obtained in place from single neutron Mutual Coulomb Dissociation events described above.

Figure 2 lists the design parameters from which we compute costs.

8 Prototype Test

The simulation studies lead to construct several prototype modules which were tested in the fall '97 run at CERN. The test was performed during the month of November as part of the NA49 run. The fall run was a proton run so that the test was performed with protons. For calibration purpouses muons were also used in the Tungsten module run.

ZDC_cost_pict_1.xls

ZDC cost estimate

Absorber parameters (tungsten):	
Absorber (W) rad. length(mm)	3.5
Absorber (W) hadron interact. length(mm)	96
Absorber density(g/cm**3)	19.3
Absorber (W) plate thickness(mm)	2.5
Number of absorb. plates in layer	2
Absorber plate width(mm)	100
Absorber plate height(mm)	150
Working absorber plate height(mm)	106.1
Working absorber plate thickness(mm)	3.536
Mass of absorber plate (kg)	0.724
Mass of absorber layer (kg)	1.448
Absorber layer sampling in X0 units	2.02
Absorber layer sampling in Lint units	0.0737
Fiber parameters (PMMA):	
Fiber diameter (mm)	0.5
Number of fiber sheets in layer	1
Effective Thickness of fibers layer(mm)	0.50
Number of fibers in layer	200
Occupied area by fibers in layer(mm**2)	50.00
Total length of all fibers in layer(m)(0.5m/piece)	100
2 -inch. diameter PMT parameters:	
Useful photocathod diameter (mm)	45
Useful photocathod area (mm**2)	1590
Number of Fiber layers may be fit(approximate)	31
Number of X0 "seen" by one PMT	62.24
Number of Li "seen" by one PMT	2.27
3 -inch. diameter PMT parameters:	
Useful photocathode diameter (mm)	65
Useful photocathod area (mm**2)	3318
Number of Fiber layers may be fit	65
Number of X0 "seen" by one PMT	132.06
Number of Li "seen" by one PMT	4.81
5 -inch. diameter PMT parameters:	
Useful photocathod diameter (mm)	110
Useful photocathod area (mm**2)	9503
Number of Fiber layers may be fit	189
Number of X0 "seen" by one PMT	381.97
Number of Li "seen" by one PMT	13.93

ZDC length (Lint)=		8
Number of layers		109
Number of absorber plates		217
Weight of absorber(kg)		157.22
Number of fiber pieces		21722
Total length of fibers (m)		10861
Total area occupied by fibers(mm**2)		5431
Length of ZDC (cm)		106
Number of 2-inch. PMT's		3.5
Number of 3-inch. PMT's		2
Number of 5-inch. PMT's		1
Cost estimation:		
Absorber @ Fibers:		
Absorber cost (at $46.00/kg)		$7,231.89
Fiber cost (at $0.50/m)		$5,430.57
Sub total price ($)		**$12,662.46**
PMTs @ bases:		
One 2" PMT(fast)($500/ea))		$500.00
One 5" PMT(free)		$0.00
2 C.-W. type bases ($100/ea)		$200.00
Sub total price($)		**$700.00**
Mechanics @ labor:		
Support/Auxiliary devices($)	$	1,000.00
Labor ($)	$	2,000.00
Sub total price($)	**$**	**3,000.00**
ZDC total price ($):		$16,362.46
Contingency (20%)		$3,272.49
ZDC gross total price:		**$19,634.95**

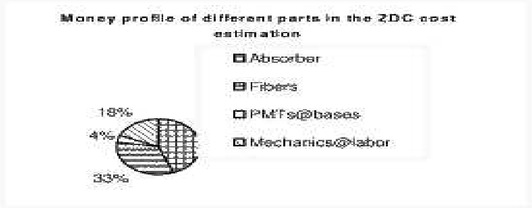

Alexei Denisov

Figure 2: Design Parameters and Cost estimate.

8.1 Tungsten Modules Testbeam Results

This is a summary of tests performed on the Tungsten modules that were prepared at BNL and tested in the NA49 beam at the end of October.

The characteristics of the prototye modules is shown in Fig. 3. The 4 modules (each 2 interaction lengths long were placed on a movable stage just upstream of the NA49 ring calorimeter. The modules were read out with 2 ". Hammamatsu PMT's (R-329-02) and their anode signals were run over 45 ft of rg-58 coax to a passive splitter which divided the signal equally between an LRS leading edge discriminator and an LRS 2249a ADC. The discriminator output was used to record time of flight in a 50 psec resolution CAMAC TDC.

For the purposes of this run beam Muons were used to obtain calibrations by adjusting the phototube gains so that muon peaks in all modules appeared in the same adc channel.

Also a measure of the photoelectron yield of each module was performed by using lineshape and assumed Poisson statistics. Alexei Denisov's tests on fiber ribbons prior to building the calorimeter gave 0.7 $p.e./mm$ of fiber thickness. Initial tests with cosmic muons at BNL also gave in the range of roughly 12 $p.e/module$. Since one module has 27 0.5 mm thick fiber layers these results are reasonably consistent.

Measurements at CERN with muons in the testbeam gave approximately 16 $pe/module$. Since the energy loss in one module is estimated to be of order 7.5 GeV it is clear that photostatistics have a negligible contribution to the module energy resolution at 100 GeV.

The PMT gain curves were measured and 2 different gain settings were established - "Channel 30" and "Channel 10" - but only the former is relevant for the data discussed below. In this exercise all modules were gain balanced using the μ peaks. Calibration energy thus has no free parameters relating the weight of depth segments. Some improvement may be possible by renormalizing to the closest calibration run. A led flasher system was also instaled. By using this system it could have been possibe to obtained the gain curves. However in the NA49 test, muon runs were available so frequently that there was no need to also take low rate led data.

8.1.1 Energy Linearity of the Calorimeter

Having preset the gains, data were taken with 100 and 160 GeV protons. The gaussian fits to the pulse height distributions at the 2 energies yield 616/380 = 1.62 shown in Fig. 4 are in excellent agreement with our expectations from linear behavior

Fitting the resolution (rms of gaussian fit) vs energy it was found a significant constant term of order 10 %. This is about the level that was found in CMS tests with copper modules with varying sampling frequency.

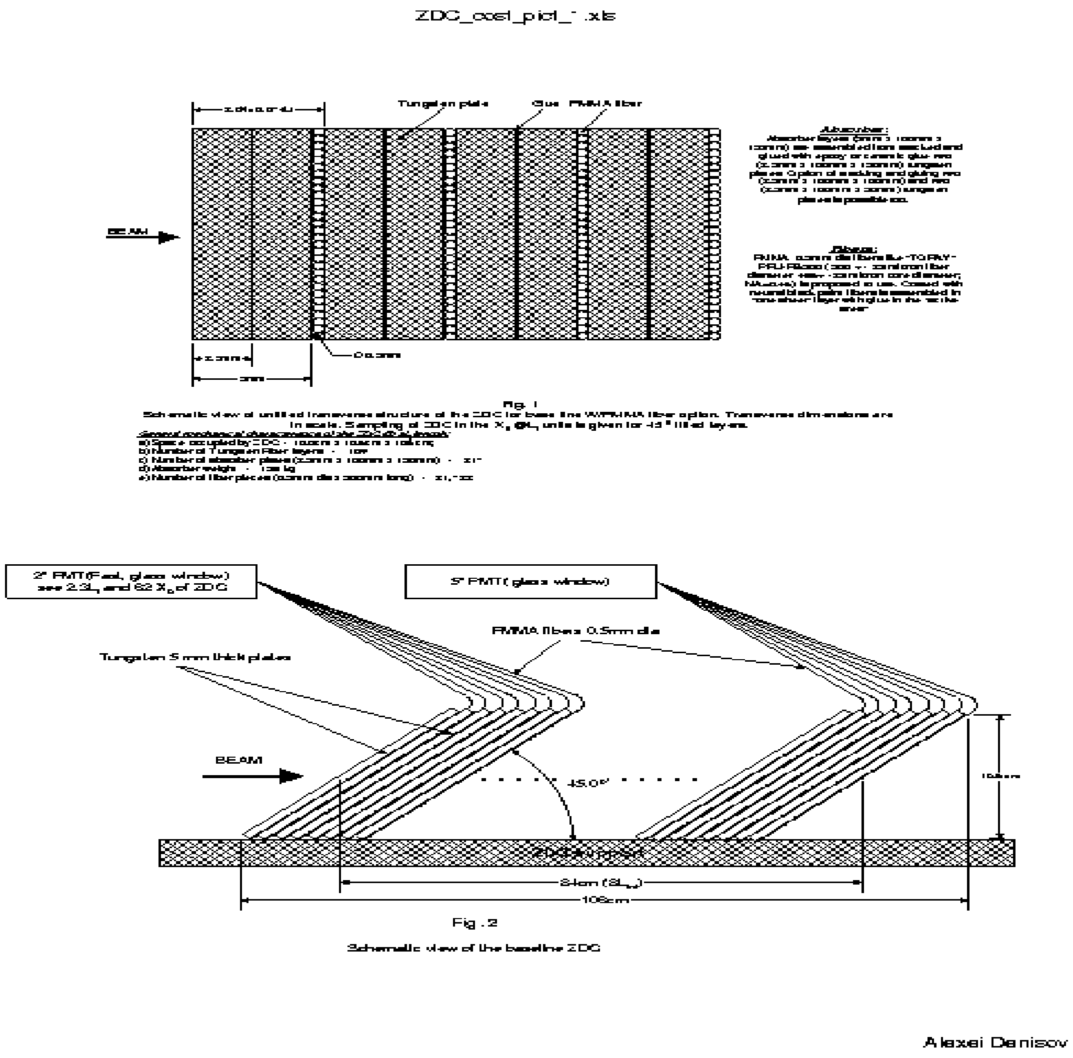

Figure 3: ZDC Design.

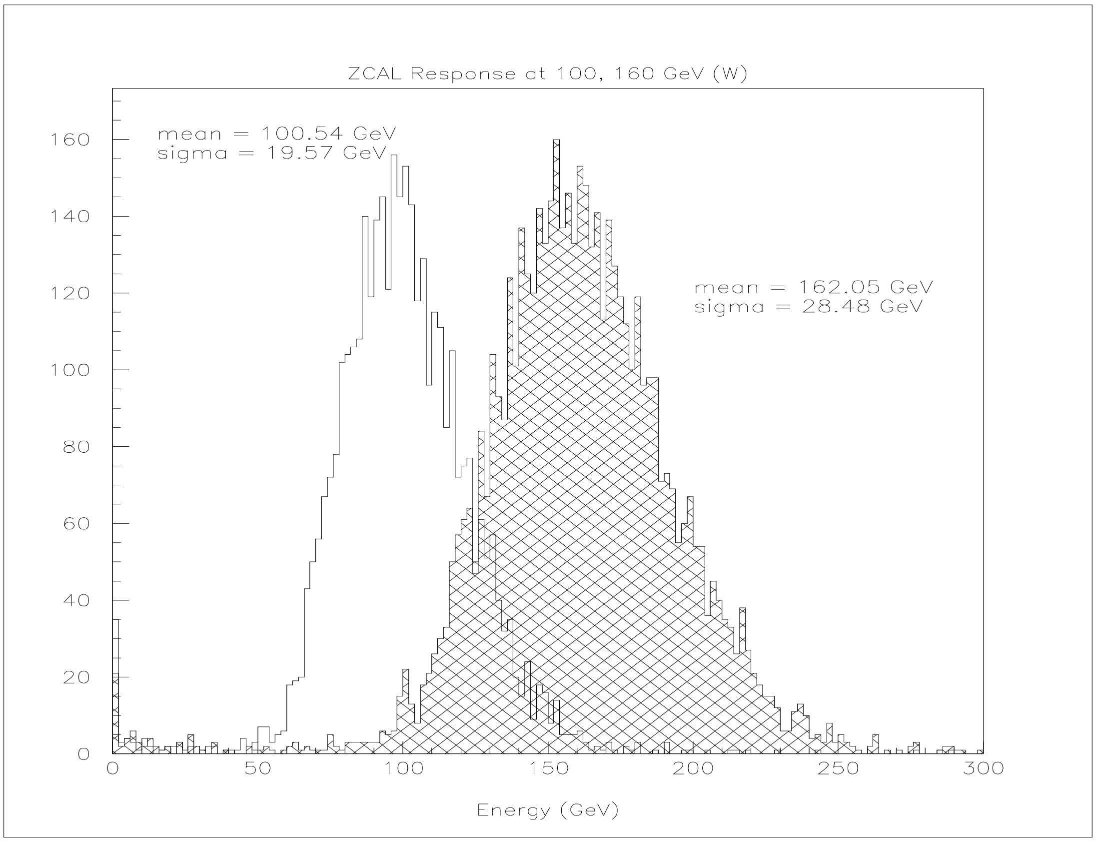

Figure 4: Energy Linearity, Tungsten Calorimeter.

8.1.2 Response map of the calorimeter

Figures 5 and 6 show variation of amplitude and sigma over the face of the detector. It is also displayed the response obtained with only 3 modules (6 lambda) and for the flipped calorimeter (where the beam was actually incident from the back of the detector). The scanning was done both along hosizontal (X) and vertical (Y) axes, of the calorimeter.

8.1.3 Timing resolution

The TOF for module 1 and 2 was slew corrected off line. Comparing to the difference between module t_1 and t_2, it was found that the start time resolution is significant and that the best resolution is that of t_1 (our first module which is 2 lambda deep) shown Fig .7. Table 1 shows the measured sigma for modules ${t_i}^m$ $i = 1, 2$, the start scintillator counter ${t_6}^m$, as well as the time differences ${t_1}^m - {t_2}^m$ and ${t_1}^m - {t_6}^m$. Table 1 shows the time resolution of the modules after the subtraction of the beam sigma σ_{t_b} Fig .8:

$$\sigma_{{t_1}^m}{}^2 = \sigma_{t_1}{}^2 + \sigma_{t_b}{}^2,$$
$$\sigma_{{t_2}^m}{}^2 = \sigma_{t_2}{}^2 + \sigma_{t_b}{}^2,$$
$$\sigma_{(t_1-t_2)^m}{}^2 = \sigma_{t_1}{}^2 + \sigma_{t_2}{}^2$$

Table 1: Measured Time resolution.

$\sigma_{{t_1}^m}$	357.5 ps
$\sigma_{{t_2}^m}$	408.90 ps
$\sigma_{{t_6}^m}$	249.50 ps
$\sigma_{(t_1-t_2)^m}$	256.5 ps
$\sigma_{(t_1-t_6)^m}$	229.5 ps

Table 2: Time resolution.

σ_{t_1}	115.0 ps
σ_{t_2}	229.0 ps

8.2 Copper Modules Testbeam Results

The copper calorimeter consisted of 8 modules which were each one interaction length (λ) long.Each module consisted of 10 layers of copper plates and fibers

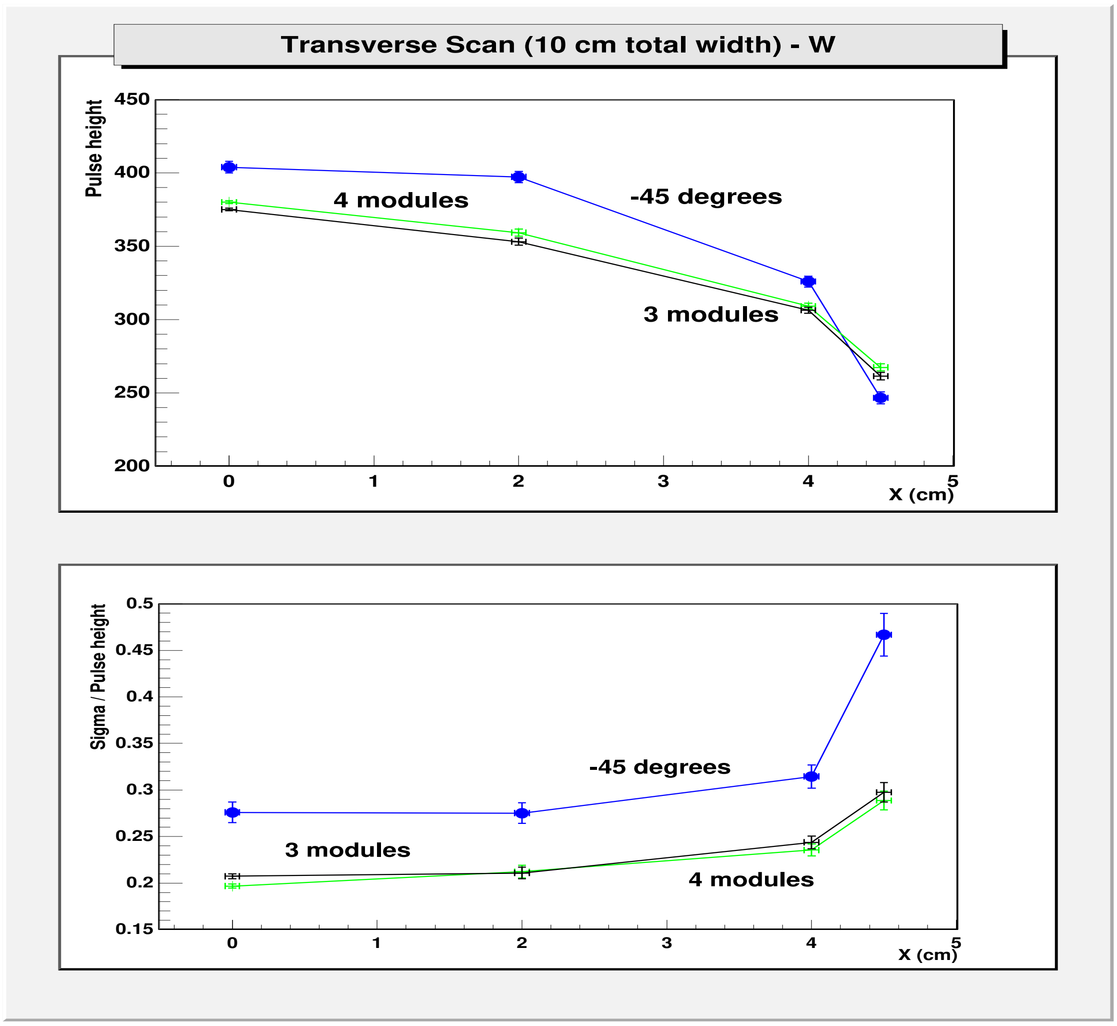

Figure 5: Horizontal scanning, Tungsten calorimeter.

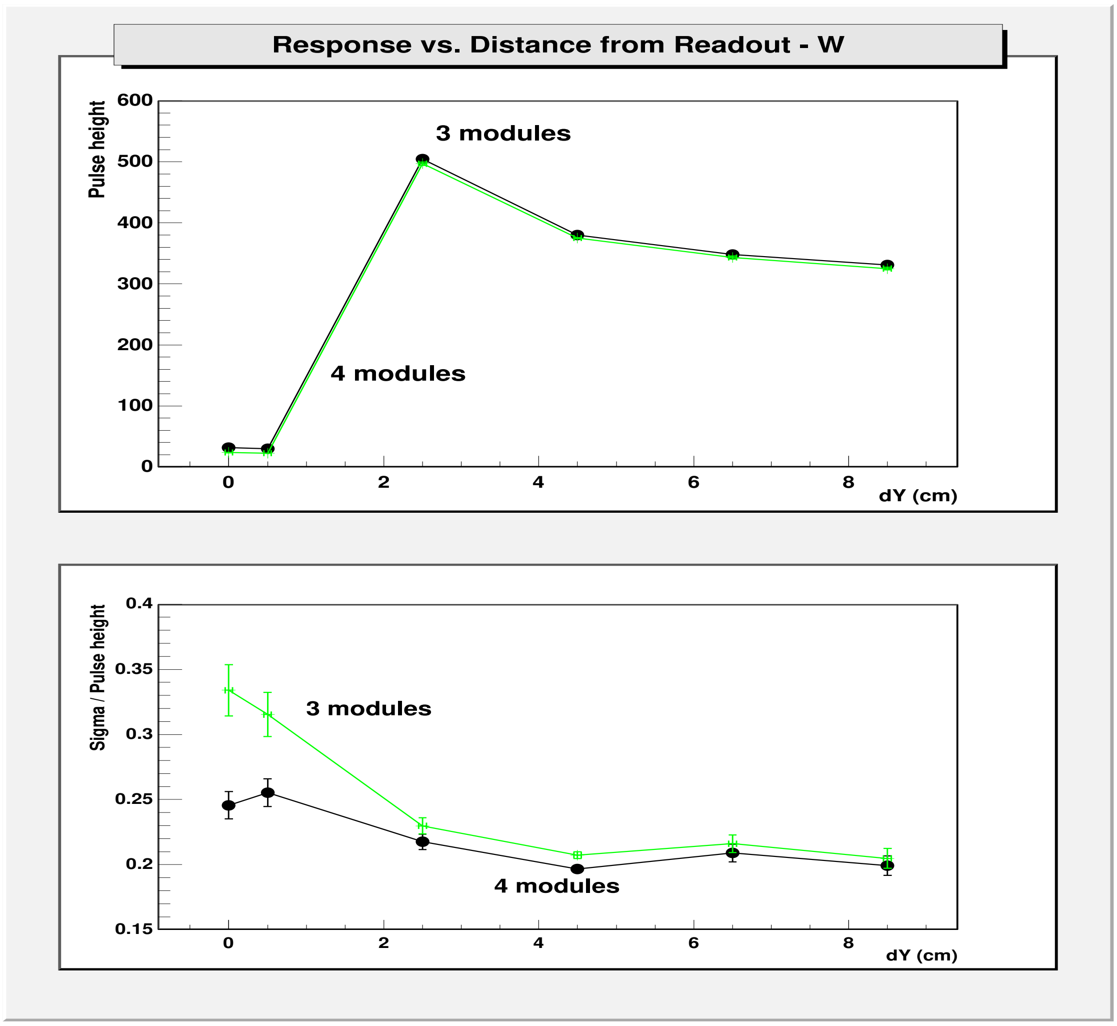

Figure 6: Vertical scanning, Tungsten calorimeter.

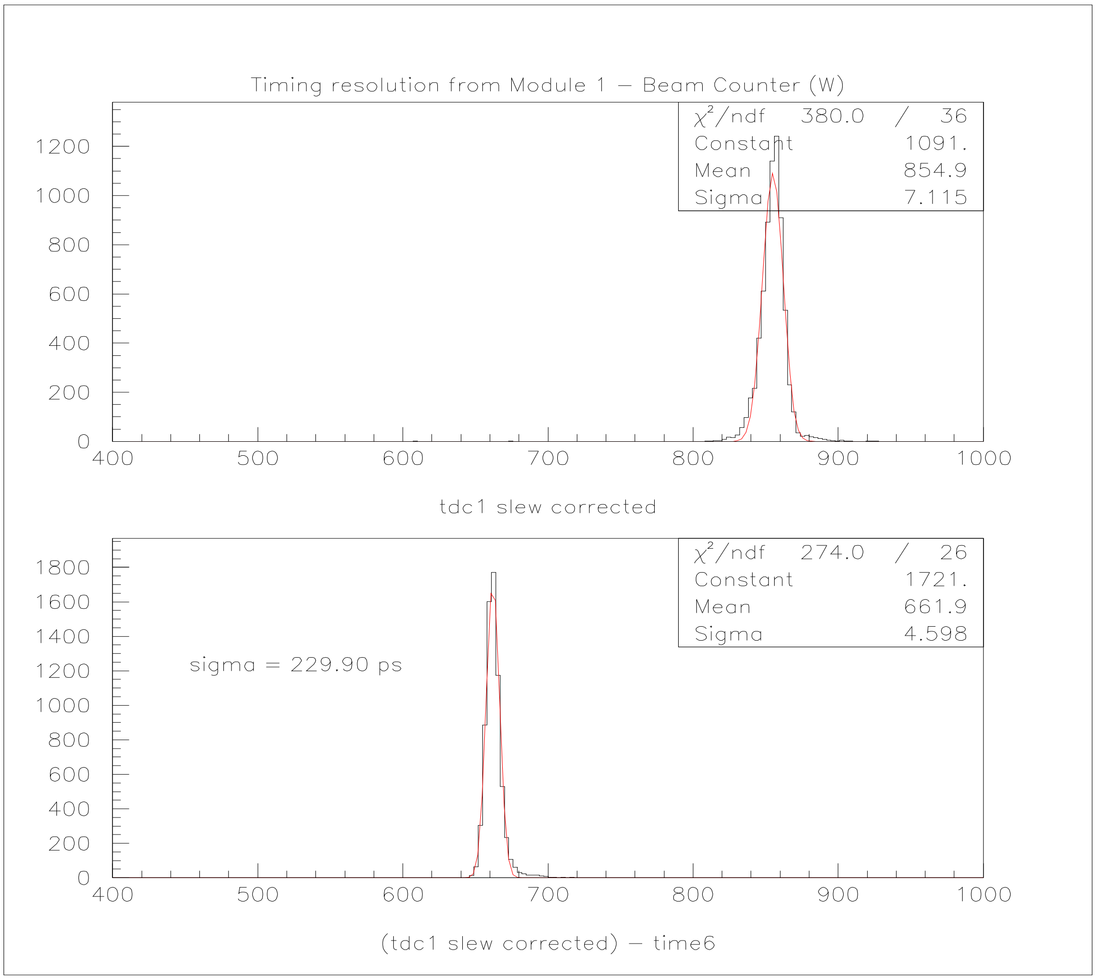

Figure 7: Timing, module 1 and 2, Tungsten calorimeter.

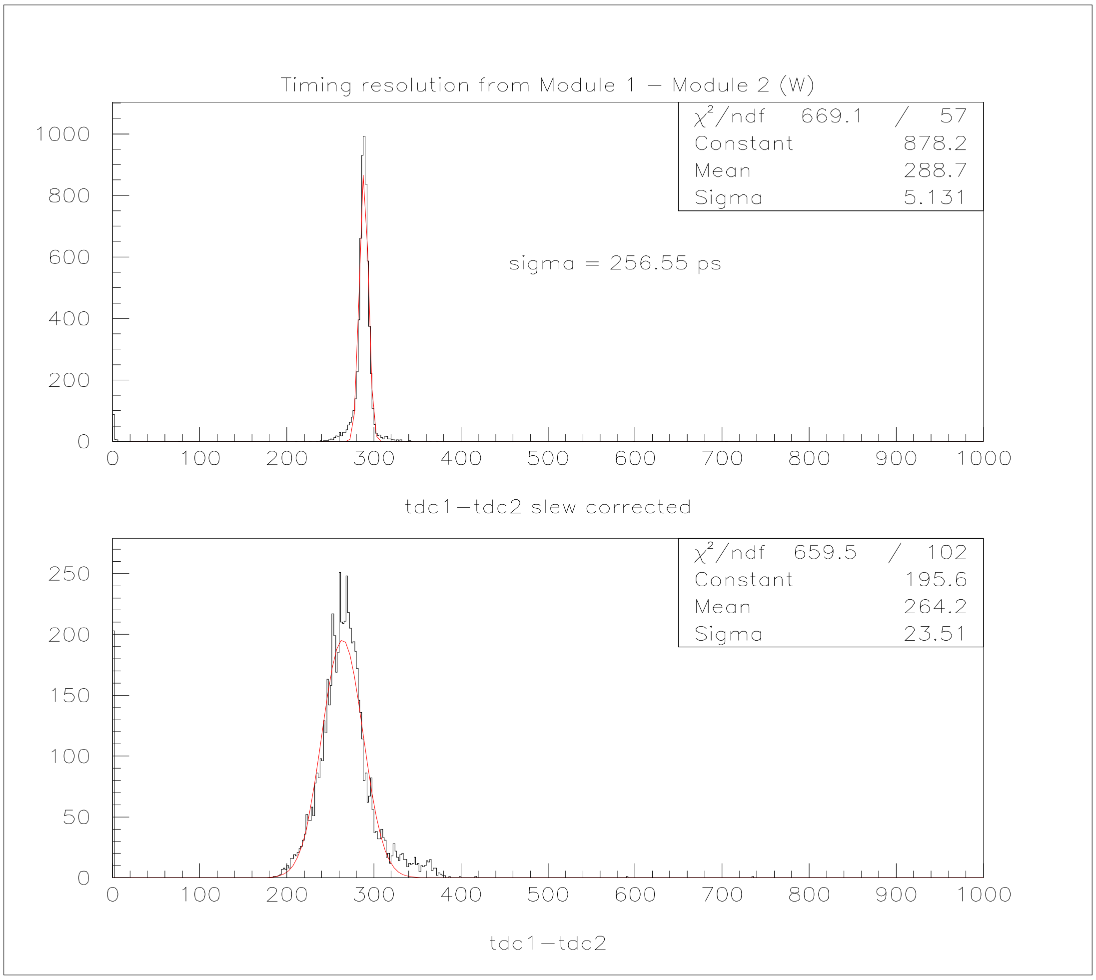

Figure 8: Timing, Module 1 and beam (counter 6), Tungsten calorimeter.

each one radiation length long and was read out by a Hamamatsu R 580-16 $1\frac{1}{2}$" photomultiplier tube.

For the energy resolution and response measurement of the copper prototype the photomultiplier signal was fed into a 10 bit charge sensing CAMAC ADC (LeCroy 2249a) read out by the NA49 data acquisition system. The data taking rate was relatively low and statistics are rather limited for the copper data. The 160 GeV/c data was taken with a faulty CAMAC crate which affected the overall gain. For this reason energy linearity of the calorimeter could not be verified.

For the tungsten prototype test and the copper timing test a faster data acquisition system was installed.The photomultiplier signals were split, one branch going into the ADC, the other into a leading edge discriminator. The discriminator signal went into an 11 bit TDC (LeCroy 2228) with the range set to 100 ns. ADC and TDC were read out via a VME OS/9 system. The data taking rate was 10 times higher than with the NA49 DAQ.

The results were compared with a GEANT simulation. The code does not include the readout system i.e. photomultipliers and fiber-photomultiplier coupling, thus photoelectrons statistic which worsens the energy resolution is not taken into account. For this reason comparison between simulated and measured data is dependent on the number of photoelectrons. The fibers above the calorimeter are bundled and bent, while in the simulation they run in straight lines as they come out of the absorber. This may produce a difference in response when the beam position is near the upper edge of the absorber.

8.2.1 Calibration

Intermodule calibration could not be done with muons, since one module has only 10 fiber layers and thus the yield was approximately 5 photoelectrons per module.Therefore we could not directly measure the amount of photoelectrons but simulation showed that the yield will be roughly the same as for the tungsten prototype i.e. 200 p.e. in all PMT's for a 100 GeV/c signal.

A coarse calibration was done online by adjusting the high voltages of the 8 photomultipliers in such a way that the longitudinal shower profile reproduced results from simulation. A further calibration was done off line by a MINUIT based program which optimized the gains of the 8 modules for minimal energy resolution.

8.2.2 Energy Resolution

Data was taken at beam energies of 160 GeV/c and 100 GeV/c. The curve shape (Fig. 9) is not Gaussian due to non-Gaussian fluctuations in the calorimeter, we will however give the values of a Gaussian fit to the curves. The resolutions obtained are 19.4$\pm$2% rms/E at 160 GeV/c and 21.4$\pm$1 % rms/E at 100 GeV/c. The values from the gaussian fit are 17.4$\pm$1% σ/E at 160 GeV/c respectively

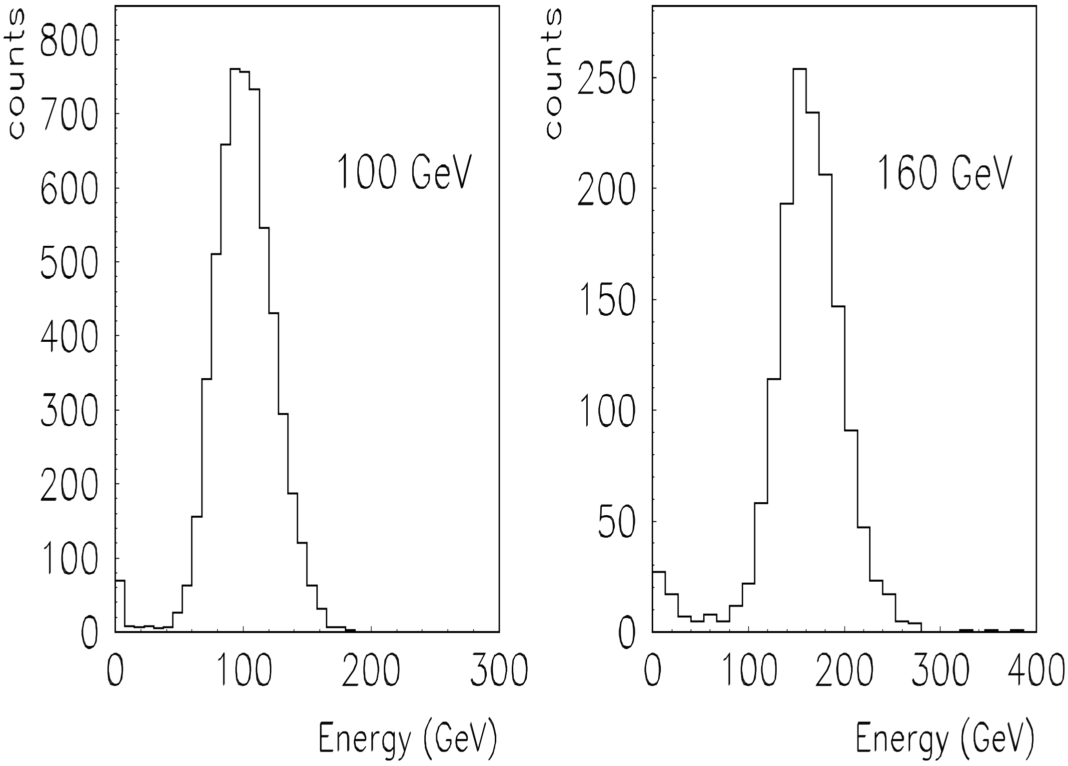

Figure 9: Response of Copper ZDC with 8 λ depth.

20.9±0.7% σ/E at 100 GeV/c. If the last two modules (absorption length) are disregarded the resolution rises to 23.5% σ/E at 100 GeV.

8.2.3 Response Map of the Calorimeter

A horizontal scan (perpendicular to the fiber orientation) with the 100 GeV/c beam was made, going from the middle of the calorimeter to both sides in 1 cm steps (Fig. 10). The result is a worsening of the energy resolution of 10% at a distance of 3 cm from the center of the calorimeter.

Simulation predicts this behavior perfectly if photoelectron statistic is included (not shown). The response falls faster than predicted by simulation if going away from the middle of the calorimeter but stays less than 5% difference within 3cm from the center.

Vertical scans (Fig. 11) reveal that for distances smaller than 2 cm from the upper edge of the calorimeter, where a significant fraction of the shower leaks into the fibers above the copper, the resolution and energy response exhibit

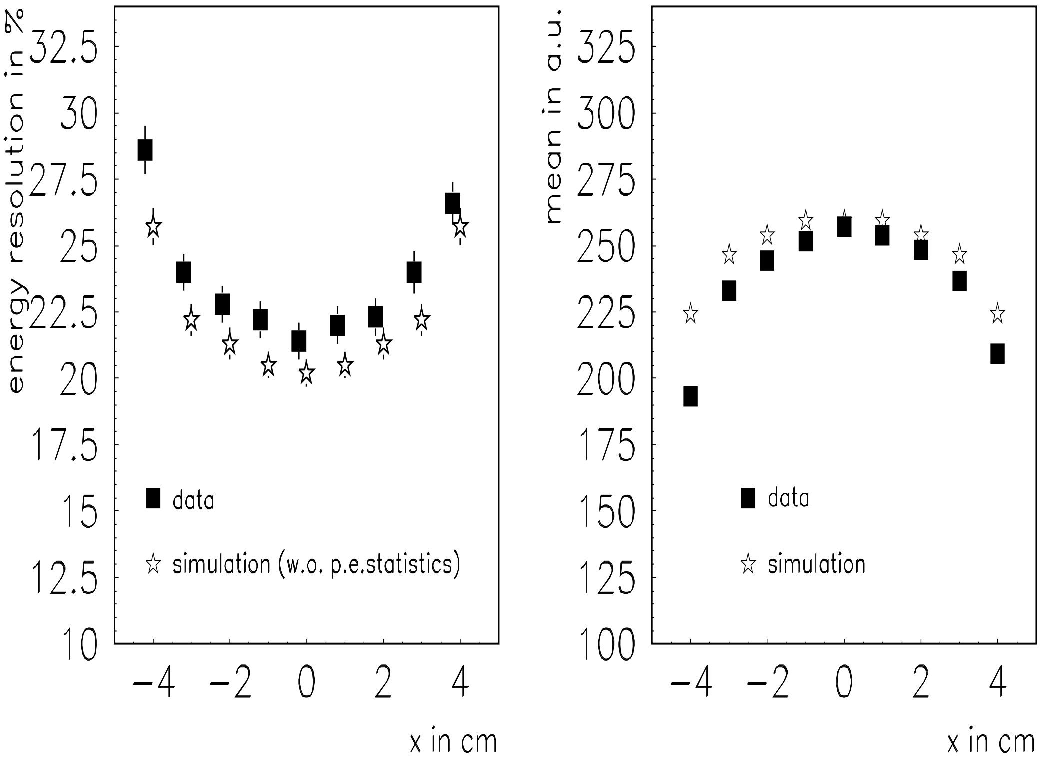

Figure 10: Horizontal scan: Energy resolution (left) and response (right). Data is compared to simulation without photoelectron statistic contribution to the worsening of the energy resolution. With 200 p.e.(beam incident in the middle of the calorimeter) the photoelectron statistic contribution amounts to 7-8 % (from middle to edges). Added squarely to the energy resolution from simulation it agrees perfectly with the data.

drastic variations. Deviations of measured data from simulation, more than 2 cm above the middle are the result of the above mentioned representation of the fibers in the simulation.

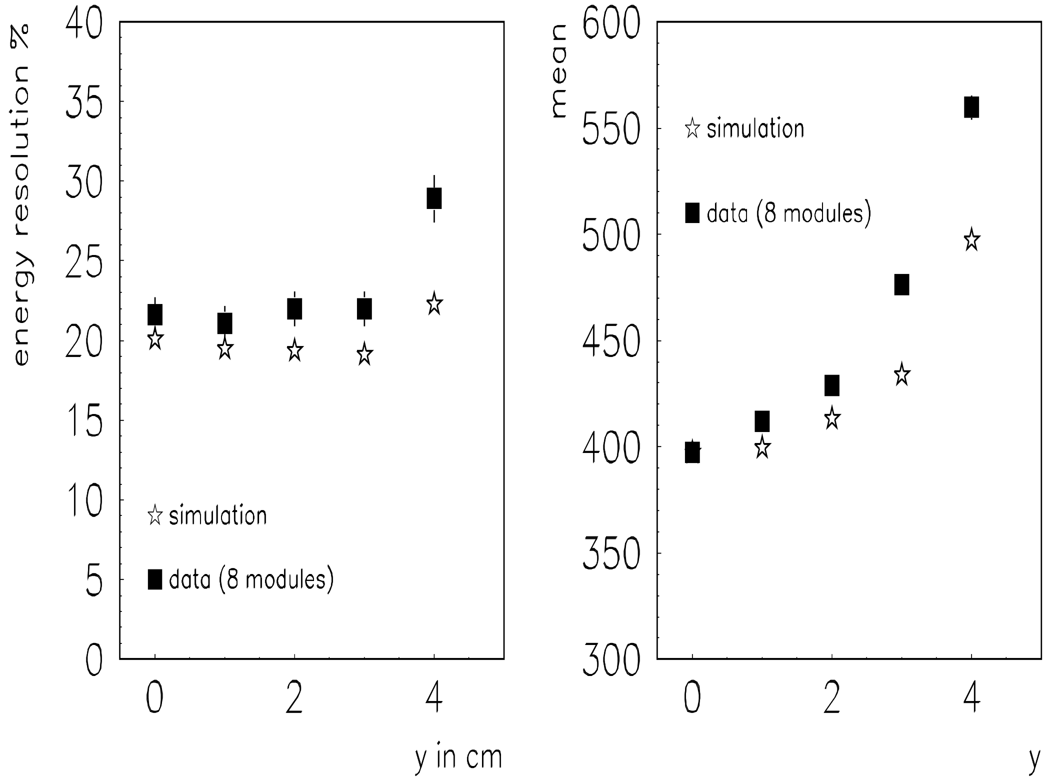

Figure 11: Vertical scan (from middle to top of calorimeter): Energy resolution (left) and response (right)

One reason to verify that the simulation reproduces the measured data, was to be able to get an answer to the question how the calorimeter behaves in the situation at RHIC where the very forward neutrons will have transverse momentum and thus have some spread over the face of the calorimeter. The single neutrons from coulomb dissociation with a maximum transverse momentum of 140 MeV/c will hit the calorimeter within 2.5 cm from the middle, which results in a energy resolution of 24 % rms/E or 23 % σ/E if a gaussian is fitted or, for the 6 module design 26 % rms/E respectively 24. 2% σ/E .

Comparison of energy resolution and response of the first 6 λ versus the whole 8 λ (Fig. 12 and fig. 13) show that the only major difference is the energy resolution which worsens about 2.5 % rms/E over the whole face of the calorimeter. Another effect of a 6 λ design is however that the low energy tail of the signal distribution is more pronounced which means, that the fraction of events that don't register in the calorimeter at all or only in the last part producing showers with a lot of longitudinal leakage and thus low signals, is increasing.

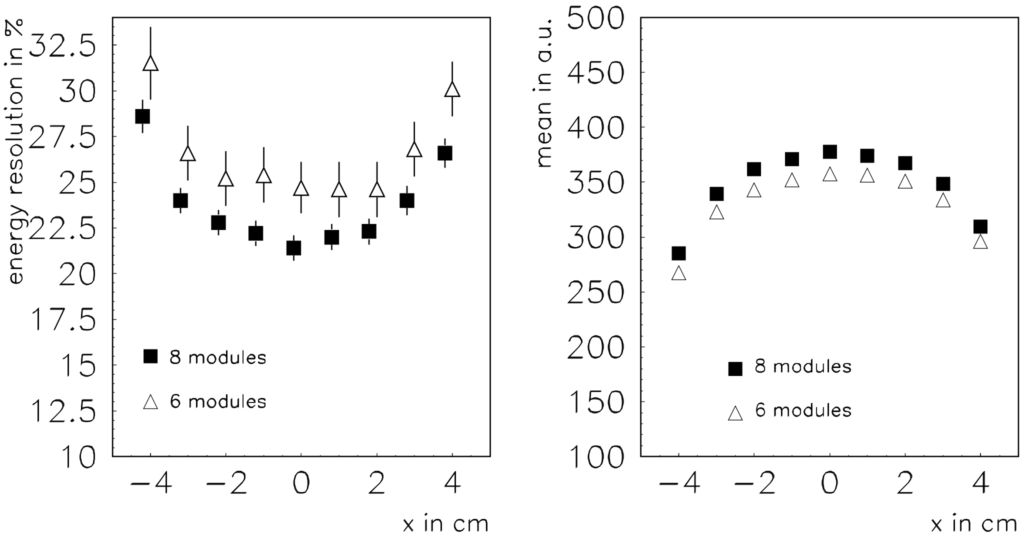

Figure 12: Horizontal scan, 8 λ versus 6 λ : Energy resolution (left) and response (right).

8.2.4 Time Resolution

Time resolution was measured together with the tungsten prototype. Only the first 4 modules were used. We used the DAQ trigger as TDC start and the signal from the modules as stop. Since the trigger was not a good absolute timing reference we also measured the time difference between the trigger and the signal from a thin fast scintillation counter in the beam line with a time resolution of approximately 100 ps.

For the determination of time resolution, a minimum signal height was required in the used module, since small signals (with only a few photoelectrons) produced bad timing due to an increase of the transit time spread in the photomultipliers. This means that a considerable fraction of the events (up to 50%) is not useful for timing information which is an important drawback compared to the design where the modules are 2 λ long.

The relative timing between modules 1,2,3 vary between 250 ps and 345 ps (Table 3). The high voltage of module 3 was 300V respectively 345V lower than

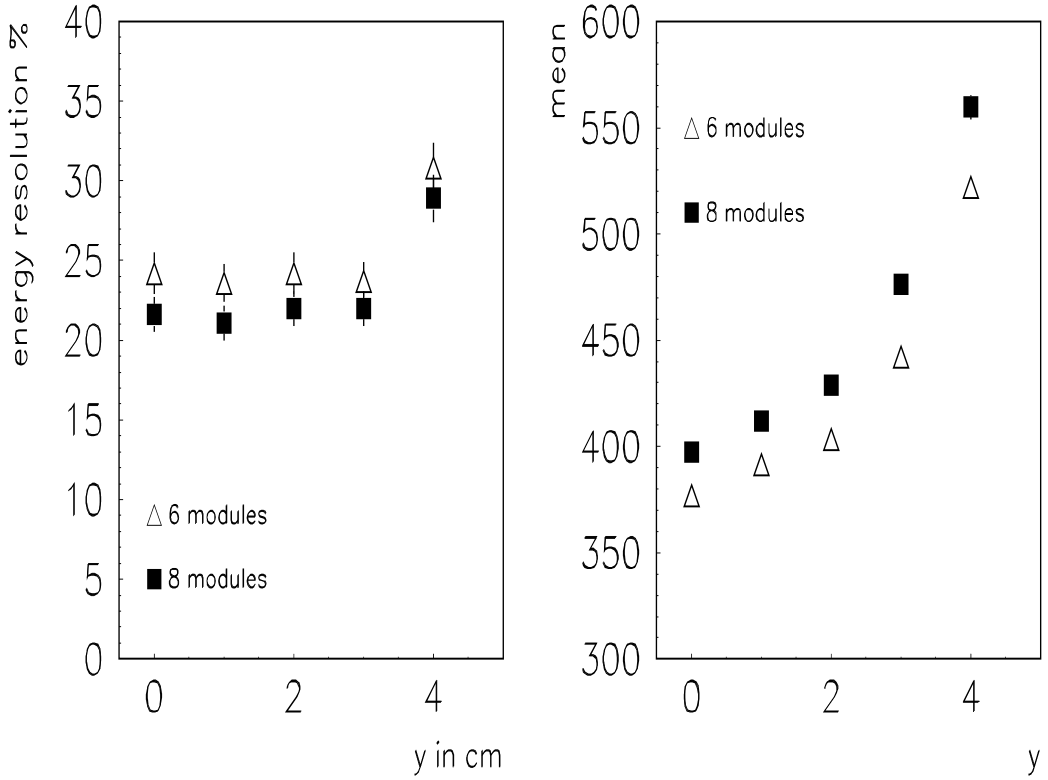

Figure 13: Vertical scan, 8 λ versus 6 λ : Energy resolution (left) and response (right).

module 1 and module 2, which is the reason for the worse time resolution with the 1-3 and 2-3 combinations.

Table 3: Relative time resolution between module 1, 2 and 3.

$\sigma_{(t_1-t_2)}$	251 ps
$\sigma_{(t_2-t_3)}$	301 ps
$\sigma_{(t_1-t_3)}$	345 ps

In order to probe the absolute time resolution of single modules they were regarded relative to the scintillation counter (Table 4). The time differences of modules 1-4 with this counter give resolutions between 230 ps and 260 ps.

Table 4: Timing resolution of module 1-4 relative to reference scintillation counter.

$\sigma_{(t_6-t_1)}$	234 ps
$\sigma_{(t_6-t_2)}$	230 ps
$\sigma_{(t_6-t_3)}$	259 ps
$\sigma_{(t_6-t_4)}$	259 ps

The best possible resolution is obtained by adding the tdc-values of module 1 and 2 and comparing the sum to the reference counter, which gives a σ of 180 ps (Fig. 15).

References

[1] A. J. Baltz and S.N.White, BNL-63127.

[2] M. J. Rhoades-Brown and J. Weneser, BNL-47806.

[3] A. J. Baltz, M. J. Rhoades-Brown, and J. Weneser, BNL-63069.

[4] T.Alber et al.(na49 collaboration) manuscript in preparation.

[5] M.Lundin et al., Nucl. Inst. and Meth. A 361 (1995) p.161

[6] D.Lazic Ph.D. Thesis "Study and Mise au point of a new calorimetry principle using Quartz Optical Fibres, Univ. Strasbourg CRN 93-38 ('95)

[7] Quartz Fibre Calorimetry-Monte Carlo Simulation, G.Anzivino et al. NIM A357 (1995) 380-385

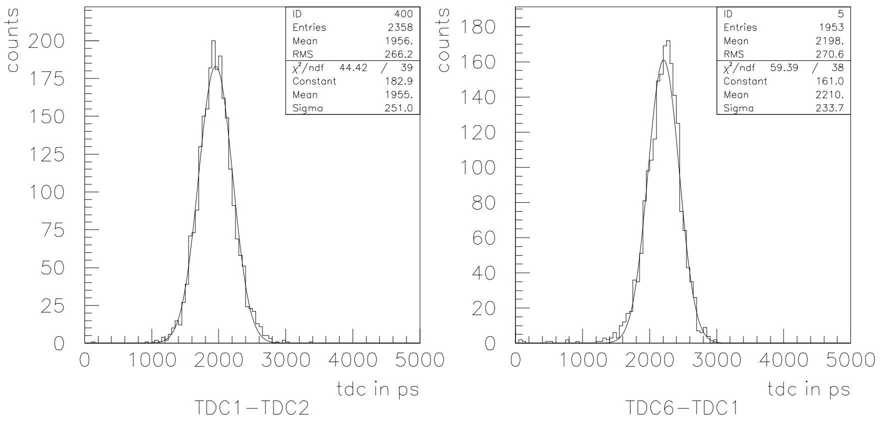

Figure 14: left: relative time resolution between modules 1 and 2, right: time resolution relative to reference counter.

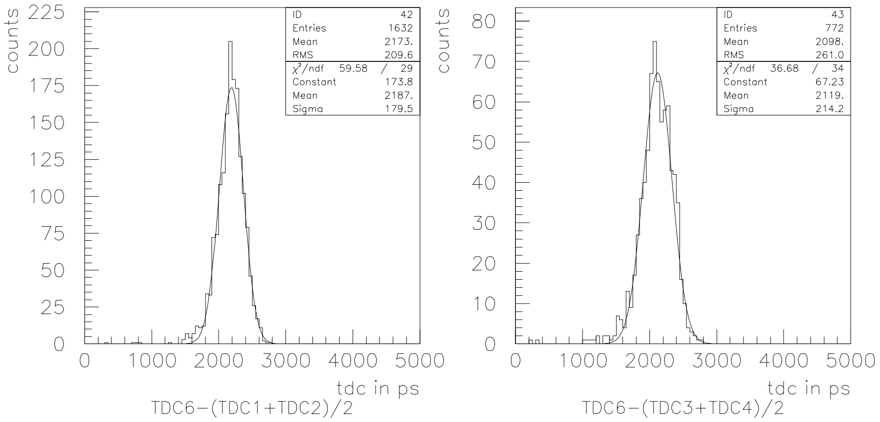

Figure 15: Adding of the signal from two modules produces best time resolution.

[8] Quartz Fibre Calorimetry for LHC experiments, O.Ganel and R. Wigmans NIM A 365(1995) 104-116

[9] On the electromagnetic Energy Resolution of Cherenkov-Fiber Calorimeters M.Lundin et al. NIM A 372(1996)359-367

[10] Quartz Fiber Calorimetry, P.Gorodetzky et al. NIM A 361 (1995)161-179 (Copper Simulation)

[11] New Results in Optical Fiber Cherenkov Calorimetry, A. Contin et al. Proceedings of 7th Vienna Wire Chamber Conference (1995)

[12] Recent Developments in Quartz Fiber Calorimetry", G. Anzivino NIM A 357 (1995) 369-379

[13] Status Report of the RD40 Project J.Britz et al. CERN/LHCC 95-27 15 April 1995

[14] 1994 CERN Test Beam Results of a 0o Fiber Cerenkov Fiber Sampling Hadron Calorimeter: A preliminary Study for CMS Very Forward Calorimetry K.Arrington et al. Dec. '94 preprint

[15] RhicDet.Note 6(http://www.rhic.bnl.gov/ rhicb/zero_degree/calorimeter.ps).

[16] J.P.de Brion- Comparative Study of Aging of PMMA and PS optical Fibers. CEN- Saclay report DPHPE 86-07(1986)

[17] Bjorken and McLerran, PRL..

[18] McLerran et al., Frankfurt preprint

[19] Jack Sandweiss, private communication. Some resulsts were presented at RHIC'97 Workshop.